Title
Assessing photochemical ozone formation in the Pearl River Delta with a photochemical trajectory model

Journal
Atmospheric Environment, 44(34)

ISSN
1352-2310

Authors
Cheng, HR
Guo, H
Saunders, SM
et al.

Publication Date
2010-11-01

DOI
10.1016/j.atmosenv.2010.07.019

Atmospheric Environment 44 (2010) 4199–4208

Contents lists available at ScienceDirect

Atmospheric Environment

journal homepage: www.elsevier.com/locate/atmosenv

Assessing photochemical ozone formation in the Pearl River Delta with a photochemical trajectory model

H.R. Cheng [a], H. Guo [a,*], S.M. Saunders [b], S.H.M. Lam [b], F. Jiang [c], X.M. Wang [d], I.J. Simpson [e], D.R. Blake [e], P.K.K. Louie [f], T.J. Wang [c]

[a] Department of Civil and Structural Engineering, the Hong Kong Polytechnic University, Hong Kong, China
[b] School of Biomedical, Biomolecular and Chemical Sciences, University of Western Australia, Perth, WA 6009, Australia
[c] School of Atmospheric Sciences, Nanjing University, Nanjing, China
[d] Guangzhou Institute of Geochemistry, Chinese Academy of Sciences, China
[e] Department of Chemistry, University of California at Irvine, CA, USA
[f] Hong Kong Environmental Protection Department, Hong Kong, China

ARTICLE INFO

Article history:
Received 9 February 2010
Received in revised form
12 July 2010
Accepted 13 July 2010

Keywords:
Master chemical mechanism
Ozone
Pearl River Delta
Photochemical ozone creation potential

ABSTRACT

A photochemical trajectory model (PTM), coupled with the Master Chemical Mechanism (MCM) describing the degradation of 139 volatile organic compounds (VOCs) in the troposphere, was developed and used for the first time to simulate the formation of photochemical pollutants at Wangqingsha (WQS), Guangzhou during photochemical pollution episodes between 12 and 17 November, 2007. The simulated diurnal variations and mixing ratios of ozone were in good agreement with observed data ($R^2 = 0.80$, $P < 0.05$), indicating that the photochemical trajectory model – an integration of boundary layer trajectories, precursor emissions and chemical processing – provides a reasonable description of ozone formation in the Pearl River Delta (PRD) region. Calculated photochemical ozone creation potential (POCP) indices for the region indicated that alkanes and oxygenated organic compounds had relatively low reactivity, while alkenes and aromatics presented high reactivity, as seen in other airsheds in Europe. Analysis of the emission inventory found that the sum of 60 of the 139 VOC species accounted for 92% of the total POCP-weighted emission. The 60 VOC species include C_2–C_6 alkenes, C_6–C_8 aromatics, biogenic VOCs, and so on. The results indicated that regional scale ozone formation in the PRD region can be mainly attributed to a relatively small number of VOC species, namely isoprene, ethene, *m*-xylene, and toluene, etc. A further investigation of the relative contribution of the main emission source categories to ozone formation suggested that mobile sources were the largest contributor to regional O_3 formation (40%), followed by biogenic sources (29%), VOC product-related sources (23%), industry (6%), biomass burning (1%), and power plants (1%). The findings obtained in this study would advance our knowledge of air quality in the PRD region, and provide useful information to local government on effective control of photochemical smog in the region.

1. Introduction

The Pearl River Delta (PRD) region is one of the most populated city clusters in China, where major cities include Hong Kong, Guangzhou, Dongguan, and Shenzhen. With its astonishing economic growth, rapid industrialization and urbanization, the region is facing more and more serious air pollution problems, such as photochemical smog, which is characterized by high concentrations of ozone (O_3) and fine particulates. Indeed, data collected at a background site (i.e. Hok Tsui) show that the O_3 levels in the PRD region increased at a rate of 0.58 ppbv year^{-1} between 1994 and 2007 (Wang et al., 2009). Elevated surface O_3 levels (above 120 ppbv) are commonly observed in autumn in the region and are of great concern due to the adverse effect on human health, visibility and global climate change (NRC, 1991; Godish, 2004). It is well documented that ground level O_3 formation is caused by reactions of the key precursors volatile organic compounds (VOCs) and nitrogen oxides (NO_x) in the presence of sunlight (Sillman, 1999). Most previous studies have shown that O_3 production is VOC-limited in the PRD region (Zhang et al., 2007, 2008; Cheng et al., 2010). For example, Zhang et al. (2008) reported that photochemical O_3 production was sensitive to VOCs at an urban site in

* Corresponding author. Tel.: + 852 34003962; fax: +852 2334 6389.
E-mail address: ceguohai@polyu.edu.hk (H. Guo).

1352-2310/$ – see front matter © 2010 Elsevier Ltd. All rights reserved.
doi:10.1016/j.atmosenv.2010.07.019

Guangzhou and a rural site, Xinken, downwind of Guangzhou. Cheng et al. (2010) also found that O_3 formation was VOC-limited at a rural site (WQS) in Guangzhou, and an urban site (TC) in Hong Kong. Hence a greater understanding of which specific VOCs contribute most to O_3 formation in the region is important for developing effective control strategies. VOCs as a group include many hundreds of species, and each one reacts at different rate and with a different reaction mechanism. For example, the initial reaction rates of VOCs with the OH radical vary by factors of 10,000, and the different molecular structures of VOCs mean that they possess intrinsically different potentials for photochemical O_3 formation. Furthermore, they are also emitted into the atmosphere at different mass emission rates, depending on the local and regional industries, land-use and biogenic sources. Hence, the relative contribution of VOCs to the photochemical O_3 formation varies from one compound to another (Atkinson, 1990; Carter, 1994) and from region to region (Derwent et al., 1996; Chang et al., 2005; Cheng et al., 2010).

To understand regional O_3 pollution and develop effective strategies to control O_3 formation, computer modeling using detailed descriptions of the chemical degradation mechanism, emission inventories, and meteorological conditions has been effectively employed (Utembe et al., 2005; Derwent et al., 2007a). A photochemical trajectory model (PTM), using the Master Chemical Mechanism (MCM), has been used to simulate photochemical O_3 formation and other secondary oxidant generated in Europe (Derwent et al., 1996, 2007a; Evtyugina et al., 2007; Pinho et al., 2009) . An index, the photochemical ozone creation potential (POCP), was developed to determine the contribution of each VOC to the regional O_3 formation in north-west Europe. The POCP for a particular VOC is determined by quantifying the effect of a small incremental increase in its emission on O_3 formation along the trajectory, relative to that resulting from an identical increase in the emission (on a mass basis) of a reference VOC, which is taken to be ethene (Saunders et al., 2003). Ethene is a suitable VOC species to normalize the POCP values because it is one of the most important O_3 precursors with medium reactivity towards hydroxyl radical, and its chemical degradation processes are also well-defined. POCPs are available in the literature from earlier studies in Europe (Derwent and Jenkin, 1991; Carter, 1994; Derwent et al., 1996, 2003, 2007a). For example, Derwent et al. (1996) described the O_3 production from the oxidation of methane and 95 other VOCs in air parcels advected across north-west Europe. Aromatic and olefinic hydrocarbons showed the highest POCP values, and halocarbons showed the lowest. Complementary work in the USA by Carter (1994) defined maximum incremental reactivity (MIR) as the amount of O_3 (grams) formed per gram of VOC emitted in an urban area. This work also suggested that aromatics and alkenes had the highest MIR values. Although regional VOC and NO_x emissions vary significantly, recently available observations and emissions inventory data coupled with the local meteorology in the PRD region have enabled the development of a detailed chemical model to assess O_3 formation in the region. For example, a number of intensive field sampling campaigns of air pollutants including O_3 and its precursors, and laboratory experiments of emission profiles of VOC sources have been conducted in the PRD region in recent years (Wang et al., 1998; Wang and Kwok, 2003; Liu et al., 2008; Zhang et al., 2008; Guo et al., 2009; Zheng et al., 2010). A detailed emission inventory of air pollutants in Asia including the study region has been developed by Streets et al. (2003) initially for the Transport and Chemical Evolution over the Pacific (TRACE-P) mission undertaken in 2000, and updated by Zhang et al. (2009) for the Intercontinental Chemical Transport Experiment – Phase B (INTEX-B) conducted in 2006. Zheng et al. (2009) recently developed a highly resolved temporal and spatial PRD regional emission inventory for 2006 with the use of newly available domestic emission factors and local activity data. These measurement data and emission inventories provide a solid base to this study for the development of a detailed chemical model in the PRD region.

A comprehensive field measurement campaign was simultaneously carried out at a non-urban site in inland PRD (WQS) and an urban site (TC) in Hong Kong from October to December 2007, in order to better understand the photochemical smog problem in this region. Using this data set, the causes of a multi-day O_3 episode were analyzed in detail (Jiang et al., 2010). In addition, the spatio-temporal variability of O_3 pollution and the impact of regional transport were overviewed (Guo et al., 2009), and the seasonal profiles and annual trends of halocarbons were examined (Zhang et al., 2010).

In this study, a photochemical trajectory model – employing the most updated version of a near-explicit photochemical mechanism (extended MCM v3.1) that describes the oxidation of methane and 139 non-methane VOCs – was developed to simulate the formation of photochemical pollutants observed at the WQS rural site in Guangzhou during a photochemical pollution episode between 12 and 17 November, 2007. The PTM was applied under a near-realistic situation in south-east China under anticyclone conditions. In this work we aimed to identify key VOC species and emission source categories that are most likely to contribute to regional scale O_3 formation in south-east China. First we compare the simulated and observed pollutant mixing ratios at three sites in the PRD, and then we simulate the reactivity of individual VOCs by calculating their individual POCP index. Finally, we identify which VOC species and emission source categories were likely to contribute most to regional scale O_3 formation in the PRD region, with the aim of assisting local management strategies and comparing with other regional airsheds.

2. Photochemical trajectory model (PTM)

2.1. Model description

The PTM is a ground level Lagrangian box model, simulating complex chemical reactions within a well mixed boundary layer air parcel, which extends from the Earth's surface up to the top of a diurnally varying boundary layer. The boundary layer height is made to vary from 300 m at night to a maximum of 1200 m during the daytime, based on radio sounding results obtained in the PRD region during the October 2004 sampling campaign (Fan et al., 2008). The horizontal dimensions of the air parcel are 3×3 km. When the air parcel moves through the pre-located trajectory, it sequentially picks up emissions from each defined grid cell of anthropogenic and biogenic VOCs, CO, NO_x, SO_2 and experiences photochemical and deposition processes. In this box model, the secondary compounds and their precursors react among themselves according to the defined chemical mechanism (i.e. MCM).

The transport process within the PTM is defined using backward trajectory path analysis. In this study, the respective backward trajectories over a 72-h period arriving at WQS, Tung Chung (TC), and Central/Western (C/W) were calculated using NOAA-HYSPLIT4.8 (Draxler and Rolph, 2003) for 1 hour intervals at the ending point of 200 m above sea level. The hourly output data of the Weather Research and Forecasting (WRF) model was used to drive the model. WRF was run in two nested domains with grid spacings of 36 km and 12 km. The finest domain covers south-east China. Grid nudging was adopted in the outmost domain to minimize integration errors. More details of the model description can be found in Jiang et al. (2008). WRF simulation was conducted for air parcel arrival times at the three sites of 0000, 0300, 0600, 0900,

1200, 1500, 1800 and 2100 hr during the period of 12–17 November 2007, with three-hour resolution for the entire sampling campaign.

2.2. Master chemical mechanism

The chemical mechanism employed in the photochemical trajectory model is an extended version of the MCMv3.1, which is a near-explicit chemical mechanism describing the detailed degradation of a large number of emitted organic compounds and the resulting generation of O_3 and other secondary pollutants under conditions appropriate to the atmospheric boundary layer (Jenkin et al., 1997). It currently describes the oxidation of methane and 139 non-methane VOCs, and contains around 13,500 reactions involving 5900 chemical species. The MCM can be accessed via the University of Leeds website (http://mcm.leeds.ac.uk/MCM).

The system of differential equations in the model is integrated with a variable order Gear's method within the FACSIMILE software suite (Curtis and Sweetenham, 1987). The initial mixing ratios for the majority of VOC species in the model are set to 0.5 ppb and, for a small number of species, initial mixing ratios are set up for typical autumn conditions associated with photochemical pollution episodes in south-east China, as follows: O_3 (20 ppbv), NO_2 (20 ppbv), CO (600 ppbv), methane (1.79 ppmv), ethane (4.0 ppbv), propane (3.5 ppbv), ethene (3.5 ppbv), propene (0.6 ppbv), ethyne (4.5 ppbv), toluene (5.0 ppbv), m,p-xylene (2.5 ppbv), formaldehyde (5.0 ppbv) (Guo et al., 2004, 2007; Barletta et al., 2005; Wang et al., 2008). In order to evaluate the impact of initial VOC mixing ratios on the model simulation results, a sensitivity test of the PTM model was carried out by setting up the initial mixing ratios of the majority of VOC species (except those list above) to each of the following values: 0.0 ppbv, 0.25 ppbv, 0.5 ppbv, 0.75 ppbv, and 1 ppbv, respectively. The percentage variation of the simulated O_3 mixing ratios was approximately 0.5–1.1% among the five different initial mixing ratios, indicating that variations in the initial modeled VOC mixing ratios have no significant influence on the simulated results.

2.3. Emission inventories

The anthropogenic emission inventory employed in this study was retrieved from the website http://www.cgrer.uiowa.edu/EMISSION_DATA_new/index_16.html, which is the INTEX-B inventory of 2006 (Zhang et al., 2009) . It is one of the most comprehensive and updated analyses of anthropogenic emissions in south-east China. The INTEX-B inventory, with a resolution of $0.5^\circ \times 0.5^\circ$ and unit of ton/year, includes six major source categories: power plants, industry, residential biofuel, residential fossil fuel, residential non-combustion, and transportation.

The biogenic VOC (BVOC) emissions used in this study are calculated from the Model of Emissions of Gases and Aerosols from Nature (MEGAN v2.04), which is defined as the MEGAN emission inventory (Guenther et al., 2006). MEGAN is a global biogenic emission model, and is designed for both global and regional emission modeling with a global coverage of about 1 km^2 spatial resolution. Only emissions of isoprene, α-pinene and β-pinene obtained from the MEGAN were used in the PTM as these three species accounted for the majority of the total BVOC emission in the region.

In addition to the above emission inventories, a 2006-based PRD emission inventory (21°27′47″–23°56′13″N and 111°59′50″–115°24′48″E, exclusive of Hong Kong and Macau) developed by Zheng et al. (2009) and an emission inventory for Hong Kong compiled by Hong Kong Environmental Protection Department (HKEPD) were also used in this study. The two emission inventories for the year of 2006, with a high resolution of 3×3 km, were compiled with newly available domestic emission factors and local activity data. These two inventories include six major categories i.e. power plants, industry, mobile sources, VOC product-related sources, biogenic sources and biomass burning.

For the target area, the allocation of total VOC emissions from a source to each VOC is obtained by applying a source profile database to each source category. The speciation profiles for each source category were drawn from two major information sources: a source profile database including vehicle exhaust, gasoline vapor, paint, asphalt, industrial and residential coal burning, biomass burning, and the petrochemical industry (Liu et al., 2008), and the USEPA SPECIATE 4.2 database (http://www.epa.gov/ttn/chief/software/speciate/, a database of total organic compounds' profiles for a variety of sources). The overall emission amount of each VOC in this study is thus obtained by multiplying the species profile of a specific source category by the total VOC emission for the same source category, and summing the emissions of the specific VOC from the major source categories. To couple with the master chemical mechanism, the anthropogenic VOC emissions from each source category were allocated to the 139 VOC species, which accounted for $93 \pm 5\%$ of the total emissions, taking into consideration that some emitted chemical species do not appear in the chemical mechanism (MCM v3.1).

2.4. Meteorological and air quality data

The main observational data used to evaluate model performance were taken at WQS in Guangzhou (Fig. 1). WQS (latitude 22°43′N, longitude 113°33′E) is a non-urban site situated at the mouth of Pearl River estuary, with the Panyu urban centre 30 km to the northwest, Dongguan city 40 km to the northeast, and Zhuhai about 50 km to the south. The sampling/measurements were conducted on the rooftop of a building in a secondary school, about 15 m above the ground level. Influence from local emissions was assumed not to be significant, largely because of the sparse population and light traffic. This site is at the geographical centre of the PRD region and downwind of the inner PRD in autumn/winter, which makes it a good location to characterize the air pollution in the inland PRD. The measurement data therefore represents the regional pollution in the inner PRD region. Further details about the site are described in Guo et al. (2009) and Cheng et al. (2010).

Air pollution data were collected at WQS from 23 October to 1 December, 2007. The measured chemical species included O_3, CO, SO_2, NO_x, and specific VOCs including carbonyls, hydrocarbons, and halocarbons. During the sampling period, ambient VOC samples were collected on selected days, i.e., 26–27 October, 13, 15–17, 23 November, and 1 December. A detailed description of the measurement techniques and VOC quality control and assurance can be found in Guo et al. (2009). For hydrocarbons and halocarbons, 102 ambient VOC samples were collected in 2-L stainless steel flasks and the mixing ratios of 61 species were quantified. For carbonyls, 32 ambient samples were collected using a carbonyl sampler (ALDEHYDE, UNIT #7) by passing air through a silica cartridge impregnated with acidified 2, 4-dinitrophenylhydrazine, and a total of 11 species were quantified. In addition to the above chemical measurements, several meteorological parameters were monitored including wind speed and direction, temperature, relative humidity and solar radiation.

To further evaluate model performance, measured data from urban Hong Kong air quality monitoring stations were also used (http://epic.epd.gov.hk/ca/uid/airdata). The selected stations were TC and C/W. TC (22°18′N, 113°56′E) is a residential site located on northern Lantau Island of Hong Kong, which is a newly-developed residential town. The C/W station (22°17′N, 114°08′E) is located at the northwest of Hong Kong Island and represents a typical Hong

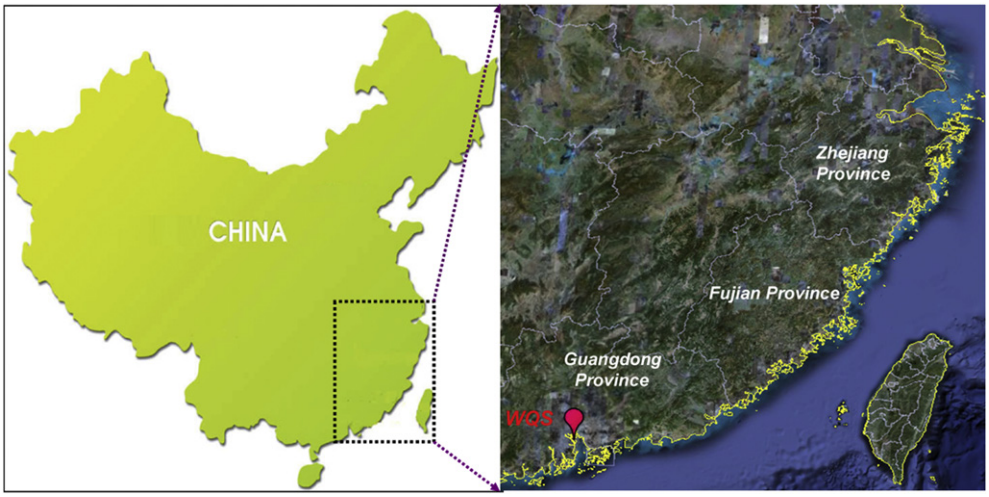

Fig. 1. Location of sampling site in Guangzhou, China (WQS).

Kong urban site, which is influenced by residential and traffic emission sources.

3. Results and discussion

3.1. Comparison of simulated and observed data

To evaluate the model performance, the simulated pollutant mixing ratios were compared with those observed at WQS (Fig. 2). The simulated NO_x showed reasonable agreement with the observed values on most of the days except on the 15 and 16 November ($R^2 = 0.44$). The observed peak NO_x mixing ratios in the morning (i.e. 8 a.m.) were 108 ppbv and 128 ppbv on the 15 and 16 November, respectively, while the simulated NO_x mixing ratios at 8 a.m. were only 51 ppbv and 63 ppbv, respectively. The difference may be attributed to chimney emissions of upwind power plants in Humen town of Dongguan, where the air masses had passed over in these two days, and/or the high vertical gradient of NO_x due to the fact that the PTM assumes that pollutants are completely mixed in the vertical direction. Another important factor for the difference may be related to the uncertainties in the 2006-based PRD emission inventory, which showed that there was medium to high uncertainty for the NO_x emission and high uncertainty for VOC and CO emissions (Zheng et al., 2009).

For O_3, the model simulated the diurnal variations very well, and the correlation coefficient (R^2) of simulated values with observed O_3 mixing ratios was 0.80 ($p < 0.05$), indicating that together the PTM and combination of boundary layer trajectories, precursor emissions and chemical processing provided a reasonable description of O_3 formation in the PRD region. However, the simulated mixing ratios were generally higher than the observed values during the sampling periods with peak value differences ranging from 0.9 to 16%, especially in the afternoon, the simulated O_3 mixing ratios did not decline as rapidly as the observed O_3

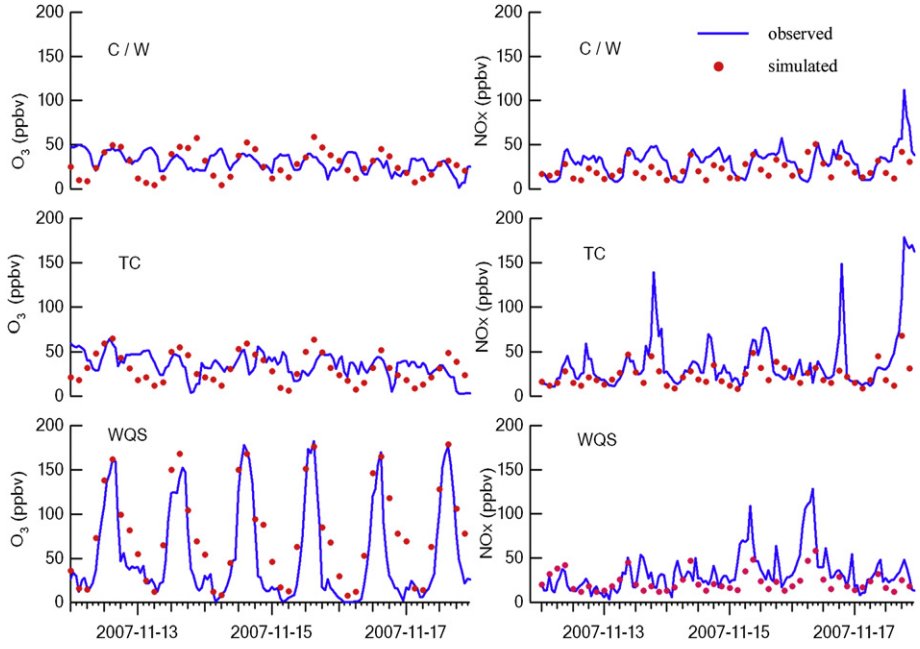

Fig. 2. Comparison of simulated (red dots) and observed (blue lines) O_3 and NO_x concentrations at WQS, TC, and C/W from November 12–17, 2007.

values. The overestimation of the simulated mixing ratios might be partially due to the fact that no horizontal dispersion was considered in this model.

The model simulation was based on the combination of the 2006-based PRD emission inventory (3×3 km), MEGAN emission inventory and the INTEX-B inventory ($0.5^\circ \times 0.5^\circ$). The simulation results using highly resolved 3×3 km emission inventory were closer to the observed data than those only based on the INTEX-B and MEGAN emission inventories (here $R^2 = 0.02$, $p = 0.31$ for NO_x, $R^2 = 0.78$, $p < 0.05$ for O_3). The large difference of predicted NO_x mixing ratios between different horizontal grid resolutions indicates that different resolutions of precursor emissions have a significant impact on model simulations.

To further evaluate the performance of the PTM, comparison of the simulated O_3 and NO_x with measured data at other locations (i.e. TC and C/W) in the PRD region during the 12–17th of November was conducted. The model simulation was generally able to capture the diurnal O_3 variations and exhibited good agreement with measurements. For example, the correlation coefficient (R^2) of simulated values with observed O_3 mixing ratios was 0.68 ($p < 0.05$) and 0.59 ($p < 0.05$) at C/W and TC, respectively (Fig. 2). During the period, the weather conditions showed a typical phenomenon which is common in the autumn season. Namely, the weather is sunny, and the sky is cloudless, and air mass movements from both North China and South China Sea are weak, which leads to a fairly stable weather system. In response to the common meteorological conditions in Hong Kong, the observed O_3 mixing ratios generally remained at a low level of about 40 ppbv at the two sites between 12 and 17 November, 2007.

In summary, the above results indicated that the PTM can provide a reasonable description of O_3 formation in both O_3 episode and non- O_3 episode days in the PRD region. It should be noted that an exact agreement between simulated and observed mixing ratios is unrealistic because of the absence of vertical and horizontal dispersion in the PTM. However, the model simulation results can guide control strategies for photochemical oxidants under typical meteorological conditions with elevated O_3 mixing ratios over PRD region.

3.2. Contribution of individual VOCs to O_3 formation

3.2.1. The base case model experiment to calculate the POCP values

Fig. 3 shows the backward trajectories of air parcels whose arrival time at WQS was 3 p.m. from 12 to 17 November, 2007. On all days the air masses originated from Zhejiang province and passed through Fujian province including Fuzhou, except for 12 November when the air mass crossed Jiangxi province including Shangrao. The air mass then passed over Guangdong province including Huizhou, Shenzhen and Dongguan, and eventually arrived at WQS on all days. Almost all the air masses had similar pathways to the receptor site during the photochemical pollution episode days when a relatively high-pressure system was formed in south-east China, corresponding to an anticyclonic flow structure over the region. This was accompanied by successive days of high temperatures (around 27 °C), long hours of sunshine, weak wind speed (lower than 1.0 m s^{-1}) and nearly cloudless skies, favorable to the formation of photochemical smog (Fig. 4). These meteorological features have been frequently associated with elevated O_3 mixing ratios in the PRD region (Wang et al., 1998; Wang and Kwok, 2003; Lam et al., 2005).

As a typical case for studying regional scale O_3 formation, a backward trajectory from 13 November (3 p.m. arrival time at WQS) was selected to determine the contribution of each VOC to the photochemical O_3 formation. This trajectory was defined as the base case experiment to calculate the POCP value of each VOC. Over

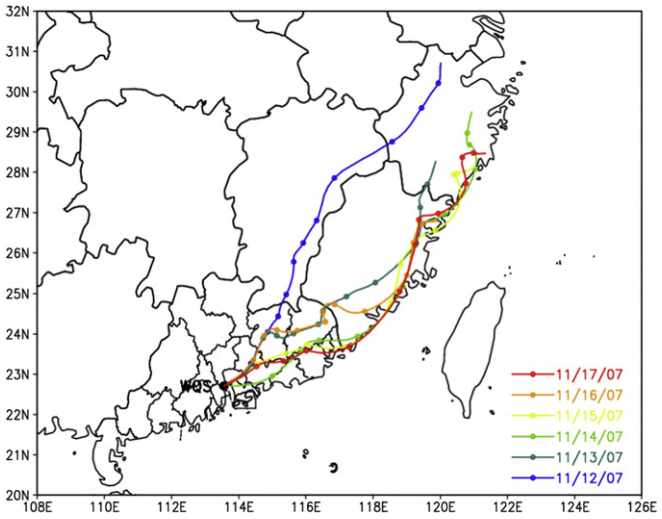

Fig. 3. Backward trajectories of air parcels whose arrival time at WQS was 3 p.m. from 12–17 November, 2007.

a 72-h period this particular air mass trajectory initialized from Lishui, Zhejiang province, passed over Fujian province including Fuzhou and Xiamen, then most parts of Guangdong province including Huizhou, Shenzhen and Dongguan, before ultimately arriving at WQS (Fig. 5). Wherever the air mass passed over, it picked up the local emissions of air pollutants. Based on the INTEX-B inventory, the 2006-based PRD emission inventory, and the MEGAN emission inventory, the time-integrated NO_x and VOC emissions for this air mass trajectory during the 72-h period were 242 and 317 kg km^{-2}, respectively.

The Photochemical ozone creation potential (POCP) concept is to provide a VOC ranking under conditions which lead to elevated ozone. Hence POCP's calculated using the base case photochemical trajectory model, would be appropriate for the region under similar conditions and can be used to describe the relative contribution of each VOC to O_3 formation at the regional scale (Section 1). The POCP for a given VOC '*i*' is defined by Eq. (1),

$$\mathrm{POCP}i = \frac{\text{ozone increment with the } i\text{th VOC}}{\text{ozone increment with the ethene}} \times 100 \qquad (1)$$

The POCP for each VOC was calculated from the result of a separate model experiment, each having the same mass increment in VOC emission (6.8% of the total integrated VOC emission across the entire model domain) above the base case experiment. The 72-h

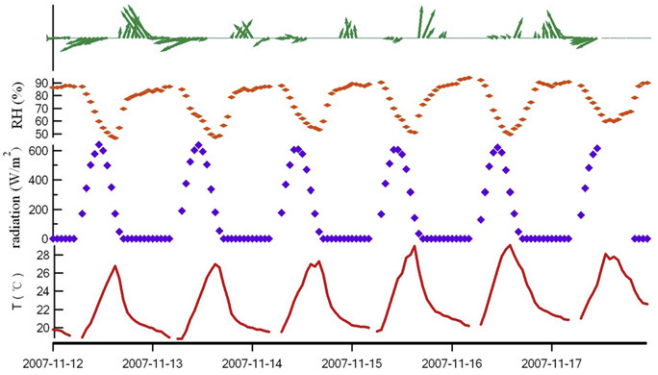

Fig. 4. Temporal variations of meteorological parameters at WQS between 12 November and 17 November, 2007.

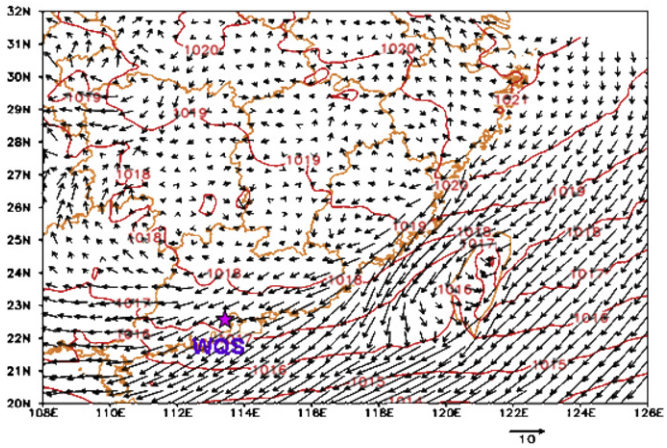

Fig. 5. Climatological chart of wind field and surface pressure at 15:00 on 13 November, 2007.

PTM was rerun 139 times, once for each VOC species described in MCM. It is noteworthy that the choice of 6.8% increase in the VOC emission was arbitrary and had no policy significance. It amounted to 21.6 kg km^{-2} in a total VOC emission of 317 kg km^{-2}. The extra VOC emission stimulated additional O_3 formation over the base case, and this incremental quantity of O_3 can be defined for a particular point along the trajectory or integrated over the entire trajectory (Derwent et al., 1996, 1998; Saunders et al., 2003).

In this study, POCP values were calculated for all 139 non-methane VOCs using the extended MCM v3.1 (Table 1). Similar to previous studies (Jenkin et al., 2003; Saunders et al., 2003), alkanes and oxygenated organic compounds have relatively low POCP values while alkenes and aromatics have high POCP values. The POCP values for alkanes ranged from 9 to 48, with ethane showing the lowest value (9). There was an increasing trend for POCP values with carbon number up to C_6, and then the POCP values remained relatively constant for carbon numbers from C_7 to C_{12}. The alkenes exhibited high POCP values, ranging from 75 (3-methyl-1-butene) to 229 (trans-2-butene). In addition, the POCP values of aromatics ranged from −85 to 197 with the highest value for 1,3,5-trimethylbenzene and the lowest POCPs (negative) for benzaldehyde and styrene. The low POCP value for benzaldehyde was likely due to its rapid photo-oxidation to nitrophenol. As a comparatively unreactive reservoir for both free radicals and NO_x, nitrophenol inhibits the O_3 formation. The negative POCP value for styrene may then also be attributed to its degradation to benzaldehyde, which is rapidly oxidized into nitrophenol (Derwent et al., 1996; Jenkin et al., 2003).

For the oxygenated organic compounds, aldehydes showed the highest mean POCP values, ranging from 30 to 116. The ethers and

Table 1
POCP values for 139 volatile organic compounds relative to ethene (=100).

VOC	POCP	VOC	POCP	VOC	POCP	VOC	POCP
Alkanes		Alcohols and Glycols		Aromatics		Chloro and hydrochlorocarbons	
Ethane	9	Methanol	11	Benzene	3	Methylchloride	1
Propane	13	Ethanol	34	Toluene	36	Methylene chloride	3
n-Butane	30	n-Propanol	41	o-Xylene	91	Chloroform	1
i-Butane	28	i-Propanol	21	m-Xylene	111	Methylchloroform	1
n-Pentane	32	n-Butanol	43	p-Xylene	88	Tetrachloroethene	2
i-Pentane	35	2-Butanol	45	Ethylbenzene	34	Trichloroethene	23
tert-Pentane	14	2-Methyl-1-propanol	38	Propylbenzene	23	cis-1,2-Dichloroethene	37
n-Hexane	36	2-Methyl-2-propanol	9	i-Propylbenzene	24	trans-1,2-Dichloroethene	34
2-Methylpentane	38	3-Pentanol	49	1,2,3-Trimethylbenzene	165	Vinyl chloride	68
3-Methylpentane	45	2-Methyl-1-butanol	46	1,2,4-Trimethylbenzene	179	1,2-Dichloroethane	4
2,2-Dimethylbutane	19	3-Methyl-1-butanol	50	1,3,5-Trimethylbenzene	197	1,1-Dichloroethene	58
2,3-Dimethylbutane	46	2-Methyl-2-butannol	22	o-Ethyl toluene	68	1,2-Dichlropropane	5
n-Heptane	40	3-Methyl-2-butanol	45	m-Ethyl toluene	85	1,1-Dichloroethane	4
2-Methylhexane	39	Cyclohexanol	65	p-Ethyl toluene	59	Chloroethane	7
3-Methylhexane	48	Diacetone alcohol	28	5-Ethyl-m-xylene	170	1,1,2,2-Tetrachloroethane	7
n-Octane	34	Propylene glycol	43	3,5-Diethyl toluene	145	1,1,2-Trichloroethane	3
n-Nonane	36	Ethylene glycol	20	Styrene	−33	Organic Acids	
n-Decane	43	Methylbutenol	46	Benzaldehyde	−85	Methanoic acid	2
n-Undecane	42	2-Butoxy Ethanol	56			Ethanoic acid	9
n-Dodecane	43			Aldehydes		Propanoic acid	13
Cyclohexane	38	Esters		Formaldehyde	67		
		Methyl formate	26	Acetaldehyde	116	Dialkenes	
Alkenes		Methyl acetate	5	Propionaldehyde	74	Isoprene	171
Ethene	100	Ethyl acetate	17	Butypraldehyde	63	1-3 Butadiene	113
Propene	160	n-Propyl acetate	22	1-Butyraldehyde	58		
1-Butene	102	i- Propyl acetate	22	Valeraldehyde	79	Monoterpenes	
cis-2-butene	216	n-Butyl acetate	22	Acryladehyde	30	α-pinene	152
trans-2-butene	229	s-Butyl acetate	29	Methacrylaldehyde	35	β-pinene	110
Isobutene	91	t-Butyl acetate	4	Crotonaldehyde	50		
1-Pentene	84					Hydrobromocarbons	
cis-2-Pentene	161	Ethers and Glycol Ethers		Ketones		Bromomethane	0
trans-2-Pentene	161	Methyl ether	26	Acetone	8	1,2-Dibromoethane	1
2-methyl-1-Butene	93	Diethyl ether	72	Butanone	28		
3-methyl-1-Butene	75	Methyl t-butyl ether	16	Pentanone	45	Other species	
2-methyl-2-Butene	202	Diisopropyl ether	54	3-Pentanone	26	Dimethoxymethane	17
1-Hexene	91	tert-Butyl ethyl ether	29	Eethyl 1-propyl ketone	33	Dimethyl carbonate	1
cis-2-Hexene	141	Methyl proxitol	58	Methyl n-butyl ketone	47	Ethylene oxide	1
trans-2-Hexene	141	Methyl glycol	38	Ethyl n-propyl ketone	45		
2-Butene	169	Ethyl glycol	54	Methyl 1-butyl ketone	65		
Alkynes		Butyl oxitol	58	Methyl t-butyl ketone	18		
Ethyne	6	n-Butoxypropanol	77	Cyclohexanone	39		

glycol ethers exhibited slightly lower mean POCPs (16–77), followed by the alcohols and glycols (9–65) and ketones (8–65). In particular, acetone, often used as a solvent, showed a remarkably low POCP value (8), indicating that it could be a potential substitute for the relatively higher reactivity aromatic VOCs in a solvent. It can be seen that esters have the second lowest mean POCP values among the oxygenated species (4–29) whereas organic acids presented the lowest values (2–13), suggesting their low contributions to O_3 formation. The halocarbons showed negligible mean POCP values (1–7), with the exception of the chloroethenes (23–68), which therefore should be considered in the assessment of target VOC reduction. The negligible POCP values of halocarbons may be attributed to their low reactivity with OH radicals and the reduced number of C–H bonds which decreased the number of HO_2 radicals formed (Derwent et al., 1996).

3.2.2. Comparison of POCPs with previous studies

Fig. 6 compares the POCP values of VOCs in the PRD region obtained by the extended MCM v3.1, with those calculated in Europe by MCM v3 (Jenkin et al., 2003; Saunders et al., 2003). There was similar general trend in VOC POCP values between the two regions, especially for alkanes and some oxygenated organic compounds like ketones and alcohols, whereby their POCP values in the two regions were almost the same. However, there were distinct differences between the PRD region and Europe for the aromatics and alkenes, with consistently higher POCP values for alkenes and reactive aromatics in the PRD than in Europe, and lower values for the least reactive aromatics in the PRD than in Europe. For example, the trans-2-butene POCP was 229 in the PRD but 111 in Europe, while those of styrene and benzaldehyde were −33 and −85 in the PRD compared to 14.5 and −10.4 in Europe. The large difference between the POCP values may be attributed to different emissions of NO_x and VOCs, variable VOC distributions and meteorological conditions such as solar radiation and temperature between the PRD and Europe. Another factor for the aromatic species may be that the mechanism used in this study (extended MCM v3.1) has been updated from that used in Europe study (MCM v3), in particular it represents aromatic degradation more completely and gives a more reasonable description of known organic product formation, even though previous studies have shown that the POCPs calculated with MCM v3.1 by Derwent et al. (2007b) are reasonably similar to those using MCM v3 by Jenkin et al. (2003) in Europe.

To further evaluate the PTM model results, we compared the POCP values obtained in this study with those predicted by the maximum incremental reactivity (MIR) method proposed by Carter (1994) from smog chamber mechanism studies (Fig. 7). In general, the POCP values showed a good agreement with the MIR values ($R^2 = 0.80$, $p < 0.05$). Both values indicated that alkenes and aromatics were the most reactive and alkanes were least reactive even though the two methods were developed for different scenarios. However, there were some remarkable differences between the two schemes. The POCP method showed that trans-2-butene was the most reactive VOC species, compared to 1,3,5-trimethylbenzene for the MIR scale. The POCP scale also showed that alkenes were stronger contributors to O_3 formation compared to the MIR method. The difference between POCP and MIR schemes is likely because the POCPs obtained in this study focused on specific regional emissions, VOC distribution and long-range transport, while the MIR method was associated with the urban scale and was developed for Los Angeles condition (Carter, 1994).

3.2.3. The Contribution of VOC species to O_3 formation

To thoroughly understand the relative contribution of each VOC to O_3 formation in the PRD region, a method combining the POCP index with the emission inventories is adopted, in which the importance of each VOC towards O_3 formation potential is ranked using its POCP-weighted emission (Table 2). In other words, the POCP-weighted value of each VOC was obtained in terms of an ethene-equivalent method (i.e. the emission of the VOC in the PRD region (kt yr^{-1}) multiplies by its POCP value/100). Based on the PRD emission inventory, the sum of the anthropogenic and biogenic VOC emissions in this region (21°27′47″–23°56′13″ N and 111°59′52″–115°24′48′E′) is 1180.1 kt yr^{-1} (Zheng et al., 2009). We used the total emission from the whole region to calculate the emissions of individual VOCs – rather than the emission in the grids where the trajectory passed over – as this would not affect the relative ranking of the VOCs in terms of their POCP-weighted value. Table 3 lists the top 15 VOCs with the highest reactivity (POCPs) and emission rates (kt/yr) in the PRD region. Trans-2-butene, cis-2-butene, 2-methyl-2-butene, 1,3,5-trimethylbenzene, 2,3-Dimethylbut-2-ene 1,2,4-trimethylbenzene, isoprene, and propene had high POCP values, while isoprene, toluene, benzene, ethene, and formaldehyde had elevated emission rates, accounting

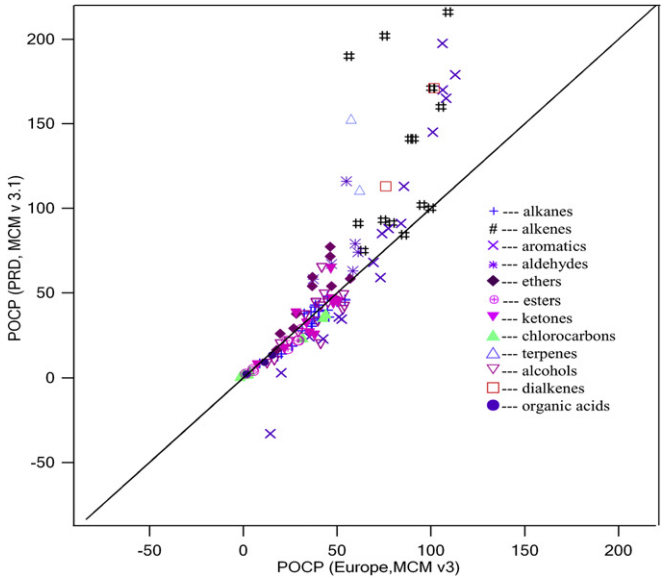

Fig. 6. Comparison of POCP values of target VOCs in the PRD region (using MCM v3.1) with those reported in Europe (using MCM v3).

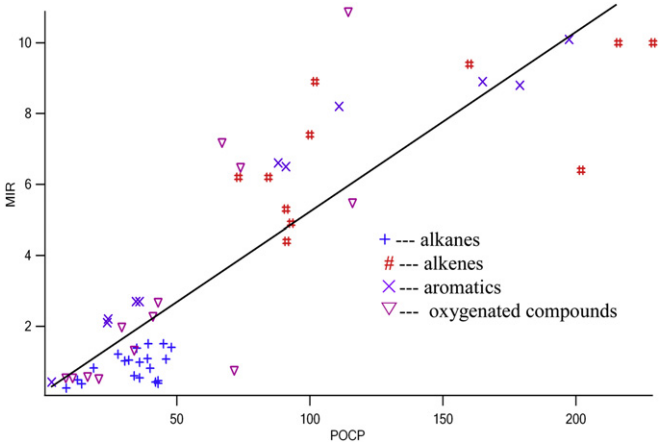

Fig. 7. Comparison of POCP and MIR values for 56 volatile organic compounds, which are available in both MCM (this study) and MIR (Carter, 1994).

Table 2
60 key volatile organic compounds included in the photochemical trajectory model together with their mass emission rates, POCPs and POCP-weighted emissions.

VOC species	Emission (kt/yr)	POCP	POCP-weighted[a]	VOC species	Emission (kt/yr)	POCP	POCP-weighted[a]
Isoprene	74.10	171	126.71	n-Hexane	7.94	36.17	2.87
Ethene	60.15	100	60.15	trans-2-Hexene	1.91	141.00	2.69
α-pinene	28.80	152	41.65	n-Butane	7.97	30.46	2.43
m-Xylene	37.45	111	43.78	cis-2-Hexene	1.64	140.88	2.30
Propene	25.59	160	41.06	i-Butane	7.81	27.58	2.15
Formaldehyde	40.92	67	27.51	2-Methylhexane	5.43	39.35	2.14
Toluene	66.93	36	24.32	Ethyne	35.92	5.90	2.12
1,2,4-Trimethylbenzene	13.55	179	24.18	3-methyl-1-Butene	2.49	74.74	1.86
β-pinene	20.80	110	19.76	trans-2-Pentene	1.09	170.72	1.86
Acetaldehyde	17.02	116	15.20	n-Octane	5.22	33.98	1.77
o-Xylene	16.73	91	22.88	3,5-Diethyl toluene	1.09	144.85	1.58
cis-2-butene	6.77	216	14.63	Propane	11.95	12.52	1.50
trans-2-butene	6.22	229	14.25	2,3-Dimethylbutane	3.16	45.76	1.44
1-Butene	13.37	102	13.69	n-Decane	3.38	42.68	1.44
1,3,5-Trimethylbenzene	5.58	197	10.97	n-Undecane	3.07	41.83	1.28
m-Ethyl toluene	11.95	85	10.17	2-methyl-1-Butene	1.09	92.51	1.01
i-Propylbenzene	42.23	24	9.99	1-Hexene	1.09	91.03	0.99
2-methyl-2-Butene	4.80	202	9.68	Isobutene	1.09	90.67	0.99
1-3 Butadiene	7.00	113	7.95	n-Nonane	2.63	36.38	0.96
1,2,3-Trimethylbenzene	4.78	165	7.92	p-Ethyl toluene	1.59	59.37	0.94
Methyl 1-butyl ketone	10.60	65	6.89	Propylbenzene	3.99	23.09	0.92
i-Pentane	16.87	35	5.90	n-Butoxypropanol	1.09	77.00	0.84
Ethylbenzene	15.93	34	5.34	Propionaldehyde	1.09	73.67	0.80
1-Pentene	6.22	84	5.25	Acetone	8.76	8.43	0.74
2-Methylpentane	13.78	38	5.23	Cyclohexanol	1.09	64.70	0.70
n-Pentane	14.13	32	4.57	1-Butyraldehyde	1.09	58.34	0.63
o-Ethyl toluene	5.58	68	3.82	2-Butoxy Ethanol	1.09	56.00	0.61
3-Methylhexane	7.17	48	3.47	Cyclohexane	1.44	38.26	0.55
Ethane	34.86	9	3.03	n-Butyl acetate	2.27	22.31	0.51
n-Heptane	7.61	40	3.02	2-Butanol	1.09	45.07	0.49

[a] Emission amount × POCP value/100.

for 7.3%, 6.6%, 6.2%, 6.0%, and 4.1% of the total emission rates, respectively. Other species, such as *m*-xylene, ethyne, and ethane also exhibited high emission rates. The most abundant 15 VOC species accounted for 54.9% of the total VOC emission rates in the PRD region.

After taking into account both photochemical reactivity (POCP) and the emission amount of each VOC, isoprene, ethene, α-pinene, *m*-xylene, propene, formaldehyde toluene, and 1,2,4-trimethylbenzene became the key emitted precursors to photochemical O_3 formation in the PRD region. The top 15 species in terms of POCP-weighted emissions contributed 74% to the O_3 formation in the region but only accounted for 43% of the total VOC emissions, suggesting that species with either high reactivity or large emissions do not necessarily have high contributions to O_3 formation. For example, trans-2-butene was the most reactive compound among the VOCs studied, but its contribution to O_3 formation only ranked twelfth due to its low emission. In contrast, ethyne and benzene accounted for a relatively high percentage of the total VOC emission (3% and 5%, respectively), yet they had negligible contribution to O_3 formation because of their low reactivity. The results imply that the emission quantity together with reactivity of individual VOCs should be considered when strategies for photochemical O_3 pollution control are formulated and implemented. Furthermore, the sum of the most abundant 60 VOC species accounted for 92% of the total POCP-weighted emission of the 139 non-methane VOCs (Table 2). The rest (79 VOCs) were either emitted in small amount or were relatively unreactive, resulting in contributions of only 8% to the total POCP-weighted emissions. The results suggest that a relatively small number of VOC species are responsible for regional scale O_3 formation in the PRD region.

Table 3
The top 15 VOCs with the highest reactivities (POCPs), and emission rates in the PRD region.

VOC	POCP	VOC	Emission rates (kt/yr)
Trans-2-butene	229	Isoprene	74.1
Cis-2-butene	216	Toluene	66.93
2-methyl-2-Butene	202	Benzene	62.90
1,3,5-Trimethylbenzene	197	Ethene	60.15
2,3-Dimethylbut-2-ene	190	Formaldehyde	40.92
1,2,4-Trimethylbenzene	179	m-Xylene	37.45
Isoprene	171	Ethyne	35.92
Trans-2-Pentene	171	Ethane	34.86
Cis-2-Pentene	171	α-pinene	28.8
5-Ethyl-m-xylene	170	Propene	25.59
1,2,3-Trimethylbenzene	165	β-pinene	20.8
Propene	160	Acetaldehyde	17.02
α-pinene	152	i-Pentane	16.87
3,5-Diethyl toluene	145	o-Xylene	16.73
Trans-2-Hexene	141	n-Pentane	14.13

The relative contribution of individual VOC species to O_3 formation in the PRD region was also investigated using an observation-based model (OBM) (Cheng et al., 2010). Both the OBM and PTM models used the same data set for model simulations. The results from both models showed that *m,p*-xylene, toluene, *o*-xylene, and formaldehyde were important precursor species to O_3 formation in the region, and that photochemical O_3 formation can be mainly attributed to a small number of VOC species. However, there were some important differences between the two modeling results. For example, POCP-weighted values using PTM showed that isoprene was the most important contributor to O_3 formation, whereas the OBM results found that isoprene had a negligible effect on the O_3 formation. The difference between the two models might be partly due to the fact that POCP-weighted values in the PTM incorporated the contributions of VOCs to O_3

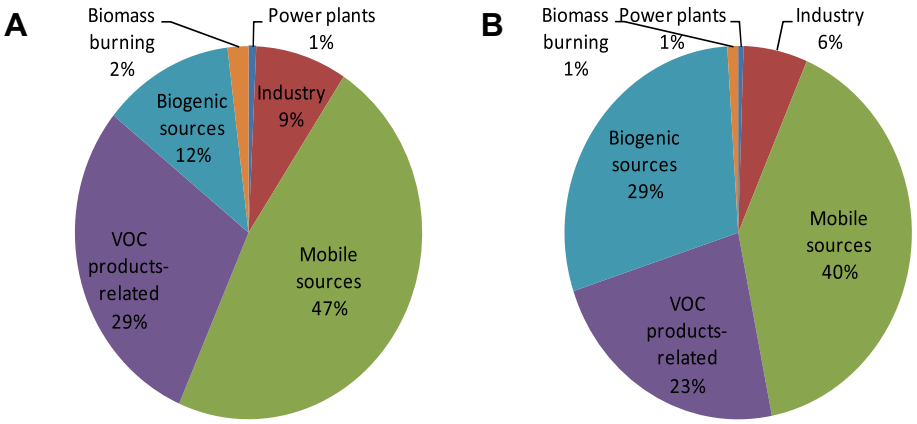

Fig. 8. Source contributions to anthropogenic VOC emissions (A) and source contributions to regional ozone formation (B).

formation at a regional scale, while the OBM results were relatively site-specific.

3.3. The contributions of VOC emission sources to O_3 formation

To determine the relative contributions of the main VOC emission source categories to O_3 formation, for a given source category each VOC's fraction by mass was multiplied by the total emission from that source category, then the emission of each VOC was multiplied by its POCP. The total POCP-weighted emissions for each source category were then summed for each VOC species, and the relative contribution of each source category to the O_3 formation was thus obtained.

Based solely on the highly resolved PRD emission inventory, mobile sources were the most important contributor to VOC emissions in the PRD region (47%), followed by VOC product-related sources (29%), biogenic sources (12%), industry (8%), biomass burning (2%), and power plants (1%) (Fig. 8). By comparison, when POCP-weighted emissions were taken into account, mobile sources remained the largest contributor to regional O_3 formation (40%), followed by biogenic sources (29%), VOC product-related sources (23%),industry (6%), biomass burning (1%), and power plants (1%). The highest contribution of mobile sources to regional O_3 formation is attributed to relatively more reactive compounds such as alkenes or aromatics present in vehicle exhaust emissions. The results also indicated that biogenic sources had a large contribution to regional O_3 formation in the PRD region.

4. Conclusions

A photochemical trajectory model (PTM), combing an updated version of the MCM, boundary layer trajectories, precursor emissions and chemical processing, was developed and employed to simulate the formation of photochemical oxidants at WQS, Guangzhou during a photochemical pollution event from 12 to 17 November, 2007. This is the first time that the photochemical trajectory model containing detailed chemical mechanism was used in the PRD region to assess the relative influence of individual VOCs to regional O_3 formation. Good agreement between the simulated and observed diurnal variations of O_3 ($R^2 = 0.80$, $p < 0.05$) suggested that the PTM simulation could provide a reasonable description of O_3 formation in the PRD region. However, the model performance of NO_x simulation was inferior and most of the observed NO_x mixing ratios were higher than the simulated values. The apparent discrepancy may be due to chimney emissions of upwind power plants in Humen town of Dongguan, and/or the high vertical gradient of NO_x, and/or the high uncertainties in the 2006-based PRD emission inventory.

Model simulations showed that alkanes and oxygenated organic compounds had relatively low POCP values while alkenes and aromatics had high POCP values. After taking into account both POCP values and emission amounts, the top 15 VOC species contributed about 74% to the total POCP-weighted emission in the PRD region, and the top 60 VOC species accounted for 92%, indicating that regional-scale O_3 formation in the PRD region can be mainly attributed to a relatively small number of VOC species. Further analysis suggested that mobile source was responsible for 40% of the regional O_3 formation, followed by biogenic sources (29%), VOC products-related (23%), industry (6%), biomass burning (1%), and power plants (1%). The results of this study should assist future policy development in targeting specific VOCs and emission source categories responsible for the air pollution episodes in the PRD region.

5. Disclaimer

The content of this paper does not necessarily reflect the views and policies of the Government of the Hong Kong Special Administrative Region (HKSAR), nor does mention of trade names or commercial products constitute an endorsement or recommendation of their use.

Acknowledgements

The authors thank Dr. Dejun Li and Mr. Zhengyue Li for their help with sample collections. The project is supported by the Postgraduate Studentship (RGYE) of the Hong Kong Polytechnic University, the Research Grants Council of the Hong Kong Special Administrative Region (Project No. PolyU 5163/07E), the Research Grant (AP0J) of the Hong Kong Polytechnic University, and the National Key Basic Research Support Foundation of China (Grant No. 2006CB403706, 2006CB403703, 2006AA06A307 and 2010CB428503).

References

Atkinson, R., 1990. Gas-phase tropospheric chemistry of organic-compounds – a review. Atmospheric Environment Part A-General Topics 24, 1–41.
Barletta, B., Meinardi, S., Rowland, F.S., Chan, C.Y., Wang, X.M., Zou, S.C., Chan, L.Y., Blake, D.R., 2005. Volatile organic compounds in 43 Chinese cities. Atmospheric Environment 39, 5979–5990.
Carter, W.P.L., 1994. Development of ozone reactivity scales for volatile organic-compounds. Journal of the Air & Waste Management Association 44, 881–899.
Chang, C.C., Chen, T.Y., Lin, C.Y., Yuan, C.S., Liu, S.C., 2005. Effects of reactive hydrocarbons on ozone formation in southern Taiwan. Atmospheric Environment 39, 2867–2878.

Cheng, H.R., Guo, H., Wang, X.M., Saunders, S.M., Lam, S.H.M., Jiang, F., Wang, T.J., Ding, A.J., Lee, S.C., Ho, K.F., 2010. On the relationship between ozone and its precursors in the Pearl River Delta: application of an observation-based model (OBM). Environmental Science and Pollution Research 17, 547–560.

Curtis, A.R., Sweetenham, W.P., 1987. FACSIMILE release H user's manual. AERE Report R11771 (HMSO), London.

Derwent, R.G., Jenkin, M.E., 1991. Hydrocarbons and the long-range transport of ozone and pan across Europe. Atmospheric Environment. Part A. General Topics 25, 1661–1678.

Derwent, R.G., Jenkin, M.E., Passant, N.R., Pilling, M.J., 2007a. Photochemical ozone creation potentials (POCPs) for different emission sources of organic compounds under European conditions estimated with a Master Chemical Mechanism. Atmospheric Environment 41, 2570–2579.

Derwent, R.G., Jenkin, M.E., Passant, N.R., Pilling, M.J., 2007b. Reactivity-based strategies for photochemical ozone control in Europe. Environmental Science & Policy 10, 445–453.

Derwent, R.G., Jenkin, M.E., Saunders, S.M., 1996. Photochemical ozone creation potentials for a large number of reactive hydrocarbons under European conditions. Atmospheric Environment 30, 181–199.

Derwent, R.G., Jenkin, M.E., Saunders, S.M., Pilling, M.J., 1998. Photochemical ozone creation potentials for organic compounds in northwest Europe calculated with a master chemical mechanism. Atmospheric Environment 32, 2429–2441.

Derwent, R.G., Jenkin, M.E., Saunders, S.M., Pilling, M.J., Simmonds, P.G., Passant, N.R., Dollard, G.J., Dumitrean, P., Kent, A., 2003. Photochemical ozone formation in north west Europe and its control. Atmospheric Environment 37, 1983–1991.

Draxler, R.R., Rolph, G.D., 2003. HYSPLIT (HYbrid Single-Particle Lagrangian Integrated Trajectory) Model access via NOAA ARL READY. NOAA Air Resources Laboratory, Sliver Spring, Maryland, USA. Website. http://www.arl.noaa.gov/ready/hysplit4.html.

Evtyugina, M.G., Pio, C., Nunes, T., Pinho, P.G., Costa, C.S., 2007. Photochemical ozone formation at Portugal West Coast under sea breeze conditions as assessed by master chemical mechanism model. Atmospheric Environment 41, 2171–2182.

Fan, S., et al., 2008. Meteorological conditions and structures of atmospheric boundary layer in October 2004 over Pearl River Delta area. Atmospheric Environment 42, 6174–6186.

Godish, T., 2004. Air Quality, 4th ed. Lewis Publishers, Boca Raton, USA.

Guenther, A., Karl, T., Harley, P., Wiedinmyer, C., Palmer, P.I., Geron, C., 2006. Estimates of global terrestrial isoprene emissions using MEGAN (Model of Emissions of Gases and Aerosols from Nature). Atmospheric Chemistry and Physics 6, 3181–3210.

Guo, H., et al., 2009. Concurrent observations of air pollutants at two sites in the Pearl River Delta and the implication of regional transport. Atmospheric Chemistry and Physics 9, 7343–7360.

Guo, H., So, K.L., Simpson, I.J., Barletta, B., Meinardi, S., Blake, D.R., 2007. C-1-C-8 volatile organic compounds in the atmosphere of Hong Kong: Overview of atmospheric processing and source apportionment. Atmospheric Environment 41, 1456–1472.

Guo, H., Wang, T., Simpson, I.J., Blake, D.R., Yu, X.M., Kwok, Y.H., Li, Y.S., 2004. Source contributions to ambient VOCs and CO at a rural site in Eastern China. Atmospheric Environment 38, 4551–4560.

Jenkin, M.E., Saunders, S.M., Pilling, M.J., 1997. The tropospheric degradation of volatile organic compounds: A protocol for mechanism development. Atmospheric Environment 31, 81–104.

Jenkin, M.E., Saunders, S.M., Wagner, V., Pilling, M.J., 2003. Protocol for the development of the Master Chemical Mechanism, MCM v3 (Part B): tropospheric degradation of aromatic volatile organic compounds. Atmospheric Chemistry and Physics 3, 181–193.

Jiang, F., Guo, H., Wang, T.J., Cheng, H.R., Ding, A.J., Wang, X.M., Simpson, I.J., Blake, D.R., Saunders, S.M., Wang, T. 2010. A photochemical smog episode in the Pearl River Delta: Field observation and model simulation. Journal of Geophysical Research-Atmospheres, in press, doi:10.1029/2009JD013583.

Jiang, F., Wang, T., Wang, T., Xie, M., Zhao, H., 2008. Numerical modeling of a continuous photochemical pollution episode in Hong Kong using WRF-chem. Atmospheric Environment 42, 8717–8727.

Lam, K.S., Wang, T.J., Wu, C.L., Li, Y.S., 2005. Study on an ozone episode in hot season in Hong Kong and transboundary air pollution over Pearl River Delta region of China. Atmospheric Environment 39, 1967–1977.

Liu, Y., Shao, M., Fu, L.L., Lu, S.H., Zeng, L.M., Tang, D.G., 2008. Source profiles of volatile organic compounds (VOCs) measured in China: Part I. Atmospheric Environment 42, 6247–6260.

Nrc, N.R.C, 1991. Rethinking the Ozone Problem in Urban and Regional Air Pollution. National Academic Press, Washington, DC.

Pinho, P.G., Lemos, L.T., Pio, C.A., Evtyugina, M.G., Nunes, T.V., Jenkin, M.E., 2009. Detailed chemical analysis of regional-scale air pollution in western Portugal using an adapted version of MCM v3.1. Science of the Total Environment 407, 2024–2038.

Saunders, S.M., Jenkin, M.E., Derwent, R.G., Pilling, M.J., 2003. Protocol for the development of the Master Chemical Mechanism, MCM v3 (Part A): tropospheric degradation of non-aromatic volatile organic compounds. Atmospheric Chemistry and Physics 3, 161–180.

Sillman, S., 1999. The relation between ozone, NOx and hydrocarbons in urban and polluted rural environments. Atmospheric Environment 33, 1821–1845.

Streets, D.G., Bond, T.C., Carmichael, G.R., Fernandes, S.D., Fu, Q., He, D., Klimont, Z., Nelson, S.M., Tsai, N.Y., Wang, M.Q., Woo, J.H., Yarber, K.F., 2003. An inventory of gaseous and primary aerosol emissions in Asia in the year 2000. Journal of Geophysical Research-Atmospheres 108.

Utembe, S.R., Jenkin, M.E., Derwent, R.G., Lewis, A.C., Hopkins, J.R., Hamilton, F.H., 2005. Modelling the ambient distribution of organic compounds during the August 2003 ozone episode in the southern UK. Faraday Discuss 130, 311–326.

Wang, J.L., et al., 2008. Characterization of ozone precursors in the Pearl River Delta by time series observation of non-methane hydrocarbons. Atmospheric Environment 42, 6233–6246.

Wang, T., Kwok, J.Y.H., 2003. Measurement and analysis of a multiday photochemical smog episode in the Pearl River delta of China. Journal of Applied Meteorology 42, 404–416.

Wang, T., Lam, K.S., Lee, A.S.Y., Pang, S.W., Tsui, W.S., 1998. Meteorological and chemical characteristics of the photochemical ozone episodes observed at Cape D'Aguilar in Hong Kong. Journal of Applied Meteorology 37, 1167–1178.

Wang, T., et al., 2009. Increasing surface ozone concentrations in the background atmosphere of Southern China, 1994–2007. Atmospheric Chemistry and Physics 9, 6216–6226.

Zhang, J., et al., 2007. Ozone production and hydrocarbon reactivity in Hong Kong, Southern China. Atmospheric Chemistry and Physics 7, 557–573.

Zhang, Q., et al., 2009. Asian emissions in 2006 for the NASA INTEX-B mission. Atmospheric Chemistry and Physics 9, 5131–5153.

Zhang, Y.H., et al., 2008. Regional ozone pollution and observation-based approach for analyzing ozone-precursor relationship during the PRIDE-PRD2004 campaign. Atmospheric Environment 42, 6203–6218.

Zhang, Y.L., Guo, H., Wang, X.M., Simpson, I.J., Barbara, B., Blake, D.R., Cheng, H.R., Saunders, S.M., 2010. Emission patterns and spatiotemporal variations of halocarbons in the Pearl River Delta region, southern China. Journal of Geophysical Research-Atmospheres. doi:10.1029/2009JD013726.

Zheng, J.Y., Zhang, L.J., Che, W.W., Zheng, Z.Y., Yin, S.S., 2009. A highly resolved temporal and spatial air pollutant emission inventory for the Pearl River Delta region, China and its uncertainty assessment. Atmospheric Environment 43, 5112–5122.

Zheng, J.Y., Zhong, L.J., Wang, T., Louie, P.K.K., Li, Z.C., 2010. Ground-level ozone in the Pearl River Delta region: analysis of data from a recently established regional air quality monitoring network. Atmospheric Environment 44, 814–823.